Materials and Design 182 (2019) 108053

Contents lists available at ScienceDirect

Materials and Design

journal homepage: www.elsevier.com/locate/matdes

# Effects of ultrasonic vibration on resistance spot welding of transformation induced plasticity steel 780 to aluminum alloy AA6061

Umair Shah, Xun Liu *

*The Ohio State University, EJTC, 1248 Arthur Adams Drive, Columbus, OH 43221, United States of America*

## HIGHLIGHTS

- In situ ultrasonic vibration enhances resistance spot welding process.
- The ultrasonic resistance welding process greatly improves Al—Fe weld properties.
- Al—Fe bonding area increases with superimposed ultrasonic.
- Ultrasonic vibration removes solidification cracking at Al—Fe interface.
- Ultrasonic vibration breaks off surface layer and promotes wetting.

## GRAPHICAL ABSTRACT

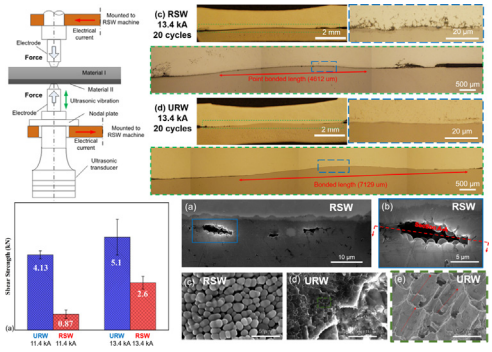


## ARTICLE INFO

*Article history:*
Received 5 June 2019
Received in revised form 28 June 2019
Accepted 17 July 2019
Available online 18 July 2019

*Keywords:*
Resistance spot welding
Power ultrasonics
Dissimilar material joining
Solidification cracking
Intermetallic compound

## ABSTRACT

A newly developed joining technique, ultrasonic resistance spot welding (URW), where high frequency ultrasonic vibration is effectively integrated into resistance spot welding (RSW) process, has been applied for joining transformation induced plasticity (TRIP) steel 780 to aluminum alloy Al 6061. Comparing URW with traditional RSW, up to 300% increase in strength and more than 150% increase in displacement to failure is achieved. Light optical microscopy (LOM) and scanning electron microscopy (SEM) revealed cracks and wide interfacial debonded regions in conventional RSW Al—Fe welds. With the assistance of ultrasonic vibrations, these interfacial cracks are effectively removed and a thin Al—Fe intermetallic layer (IMC) of around 3 um thickness is formed. SEM images of the fractured surface revealed that ultrasonic waves eliminated the eggcrate morphology generally observed in RSW welds fractured surface, which is a typical representative of solidification cracking. In situ high speed videos showed that ultrasonic vibration can help break off surface contamination and oxides as well as improving wetting of melted aluminum over the Al—Fe interface.



## 1. Introduction

Resistance spot welding (RSW) has been extensively used in automobile industries based on its high level of productivity and degree of automation. During the process, large electrical current flows through the material to generate resistance heating, particularly at the contact interface. Fusion occurs and a weld is created after solidification. Despite its widespread applications, RSW is difficult to join aluminum to steel. This is on one hand due to the large differences in physical and mechanical properties between these two materials. The electrical and thermal conductivity of aluminum is much higher than steel while the aluminum melting point is less than half that of steel. A slight adjustment of electrical current density can easily induce undesirable aluminum

* Corresponding author.
*E-mail address:* liu.7054@osu.edu (X. Liu).

https://doi.org/10.1016/j.matdes.2019.108053

expulsion. Moreover, brittle intermetallics (IMCs) are formed due to poor metallurgical compatibility and limited mutual solubility between Al and Fe. With the growing use of advanced high strength steels, dissimilar Al-steel RSW joining has become more challenging. Several attempts have been made to improve the weldability, including preheating of the workpiece [1], optimization of process parameters and electrode dimensions [2], novel design of electrode morphology (e.g. the Multi-Ring Domed electrode from the General Motor [3]), and placing additional steel cover plate on top of aluminum to control the heat balance [4]. However, despite these efforts, there are always limitations in certain aspects.

On the other hand, ultrasonic welding (UW) shows several superiorities over RSW in welding dissimilar materials as a solid-state process. During UW of metals, ultrasonic vibration (typically 20 kHz) is applied parallel to the interface. Friction oscillations generate heat and abrade off surface oxide layers and contaminations. This brings the material nascent surface into intimate contact under pressure and achieves metal bonding without melting. UW is highly energy efficient (0.6–1.5 kJ/weld) and has a minimal heat affected zone [5]. Haddadi et al. reported a maximum strength of 3 kN with button pullout failure mode for aluminum to steel ultrasonic welds [6]. Despite these advantages, current applications of UW are restricted in thin gage sheets and soft materials due to the limited allowable power of generally available ultrasonic transducers.

In this study, a new ultrasonic resistance welding (URW) process is developed, which utilizes advantages of both RSW and UW. In this process, RSW is integrated with UW through in situ application of perpendicular ultrasonic vibrations at the weld interface. This hybrid process has been applied for joining aluminum alloy AA6061 to TRIP steel and showed superior properties compared with conventional RSW welds.

## 2. Experimental details

Commercially available Al-6061T6 (McMaster) and electrogalvanized TRIP-780 (ArcelorMittal) with dimensions of $70^{L}x25^{W}x1.6^{T}$ mm$^3$ and $70^{L}x25^{W}x1.3^{T}$ mm$^3$ respectively are used in this study. The design of the URW system is based on an RSW machine and a schematic illustration is provided in Fig. 1(a). AC current passes from the top to the bottom electrode, which is connected to the ultrasonic transducer serving as the sonotrode to transfer acoustic energy into the workpiece. The total length of the bottom electrode is tuned such that its surface vibrates at the maximum displacement with a natural frequency resonating with the ultrasonic transducer (19.4 kHz). The tip diameter of top and bottom electrode is 10 mm. The electrical current is measured via a Rogowski coil and the dynamic welding force is measured through a highly sensitive strain sensor (Kistler 9232A) installed under the lower arm of the RSW machine. A self-developed LabView program digitally controls the start-and-off time of the ultrasonic power generator. In this study, the ultrasonic vibration starts after 3 cycles of AC current and continues for a duration of 167 ms (peak to peak vibration amplitude 34 μm). Other investigated welding parameters are summarized in Table 1, where the magnitude of the AC electrical current is shown with the root mean square (RMS) values. These parameters are selected based on welds with acceptable properties. Each

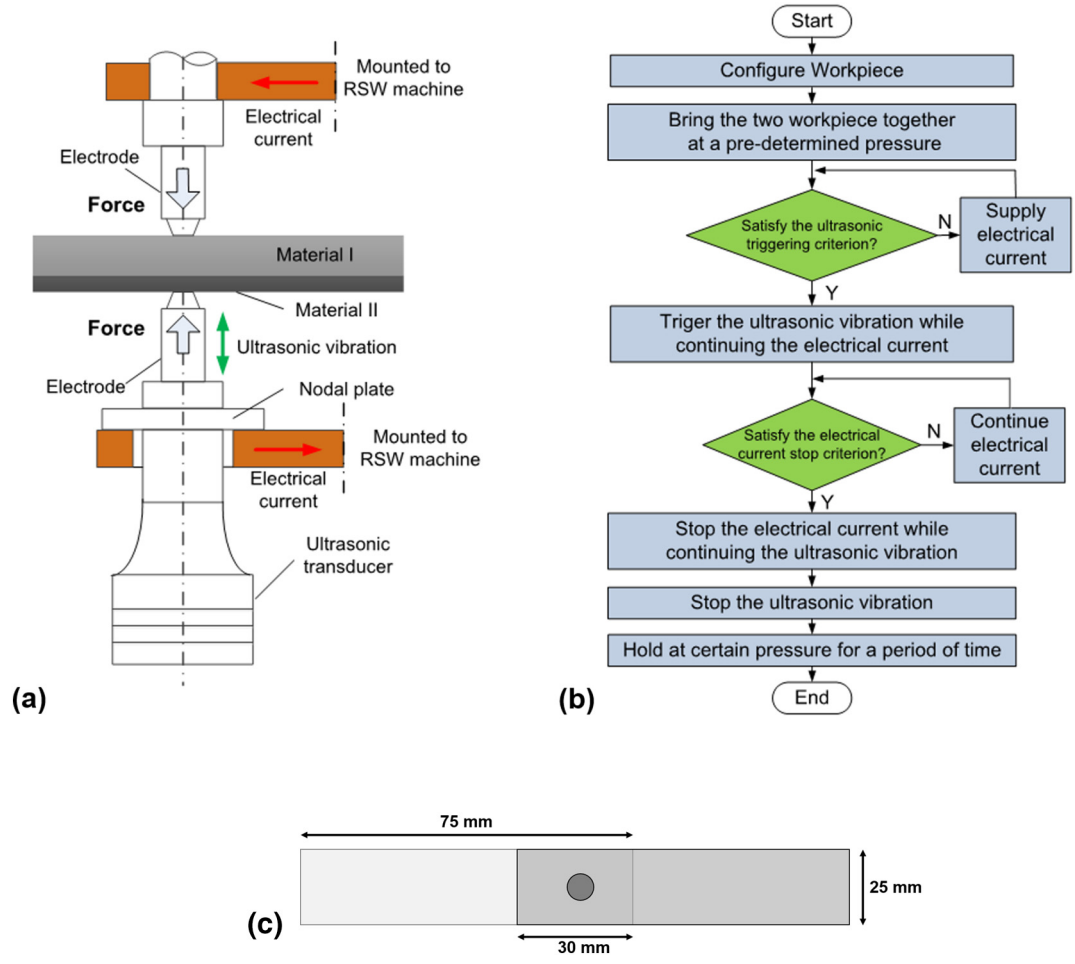


**Fig. 1.** URW Setup (a) Schematic illustration; (b) Flowchart of the URW process; (c) Geometry of the welded specimen for lap shear tensile test.

**Table 1**
RSW and URW conditions (Note: force refers to the applied welding force, which varies dynamically during the process.

| No | Material | Thickness | Current (RMS) | Current Cycles | Force | Condition |
|---|---|---|---|---|---|---|
| 1. | Al-6061 | 1.6 mm | 11.4 kA | 30 c @60 Hz | ~3.2 kN | RSW |
| | Trip-780 | 1.3 mm | | | | |
| 2. | Al-6061 | 1.6 mm | 11.4 kA | 30 c @60 Hz | ~3.2 kN | URW |
| | Trip-780 | 1.3 mm | | | | |
| 3. | Al-6061 | 1.6 mm | 13.4 kA | 20 c @60 Hz | ~3.2 kN | RSW |
| | Trip-780 | 1.3 mm | | | | |
| 4. | Al-6061 | 1.6 mm | 13.4 kA | 20 c @60 Hz | ~3.2 kN | URW |
| | Trip-780 | 1.3 mm | | | | |

condition is repeated for a minimum of 5 times. Lap shear tensile tests were performed via MTS 800 test machine at a rate of 1 mm/min and the detailed specimen dimensions are provided in Fig. 1(c). Regarding weld cross section characterizations, the Al—Fe interface is examined via Quanta-200 scanning electron microscope (SEM). EDS line scans are performed via EDAX 102 mm Octane Prime EDS detector with accelerating voltage of 14 kV, step size of 0.2 μm and a total scanning distance of 20 μm.

## 3. Results

Fig. 2 (a) shows the recorded welding force during RSW at 13.4 kA for 20 cycles. Initial variations in the curves are due to the deformation of material surface asperities as the two substrates start to contact each other. As the welding current passes through, oscillations are observed, which matches the AC current waveform. This is because the material deformation resistance can be reduced by electrical current through direct electro-plastic effect (EPE) [7] and indirect thermal softening from resistance heating. EPE has been shown on various metals and alloys, where a drop of material flow stress is observed when high density electrical current is passed through during plastic deformation. Different mechanisms have been proposed to explain this EPE effect. One hypothesis is that as the electrons pass through the deformation region, associated energies of moving electrons are transferred into dislocations, which facilitate their motion and modify the dislocations multiplications and arrangements [8]. As the absolute value of electrical current reaches the peak magnitude, the material is softened to the highest degree, which is reflected as a valley on the welding force curve. Certain large spikes are observed, indicating expulsion since the material flow stress will drop dramatically as they get melted. After the current is stopped, the force curve is slightly lower than the original level, which is possibly due to the reduced sheets total thickness after they were plastically deformed at high temperature [9].

Large oscillations of welding force can be observed during URW process in Fig. 2(b). The oscillation starts after about 3 cycles of AC current, as shown in the force and current waveform. This could be attributed to the superimposed dynamic stress induced by ultrasonic vibrations [10]. In addition, ultrasonic energy creates a softening effect similar to EPE in metals known as acoustic plastic effect (APE). During plastic deformation, the ultrasonic vibration interacts with material in terms of internal friction and dislocation movements [11]. Local absorbance of ultrasonic energy at the dislocations sites, dislocation annihilation and stress superposition result in reduction of material deformation resistance and potentially additional residual softening [12]. This acoustic softening is also reflected as variations on the welding force curves in Fig. 2 (b). A fast Fourier transformation analysis reveals a peak at the frequency of 19.7 kHz, which is slightly higher than the ultrasonic frequency measured in the unloaded condition (19.4 kHz). Another peak of 120 Hz also shows up, representing cycles of the absolute AC current values.

### 3.1. Mechanical properties comparisons

Fig. 3 compares the mechanical behavior of URW and conventional RSW welds during lap shear tensile tests. At 11.4 kA and 30 cycles, 300% increase in joint strength is achieved after applying high-frequency ultrasonic vibration. Similarly, in the case of 13.4 kA and 20 cycles, up to 90% increase in strength is obtained. Total energy absorption of URW welds (Fig. 3b) is much higher than that of RSW welds, i.e. ~713 N-mm at 11.4 kA and ~1749 N-mm at 13.4 kA condition. This is also reflected from the much larger area under the load-displacement curves of URW joints (Fig. 3c &d), showing a greatly enhanced load-bearing capacity. At 11.4 kA, interfacial failure

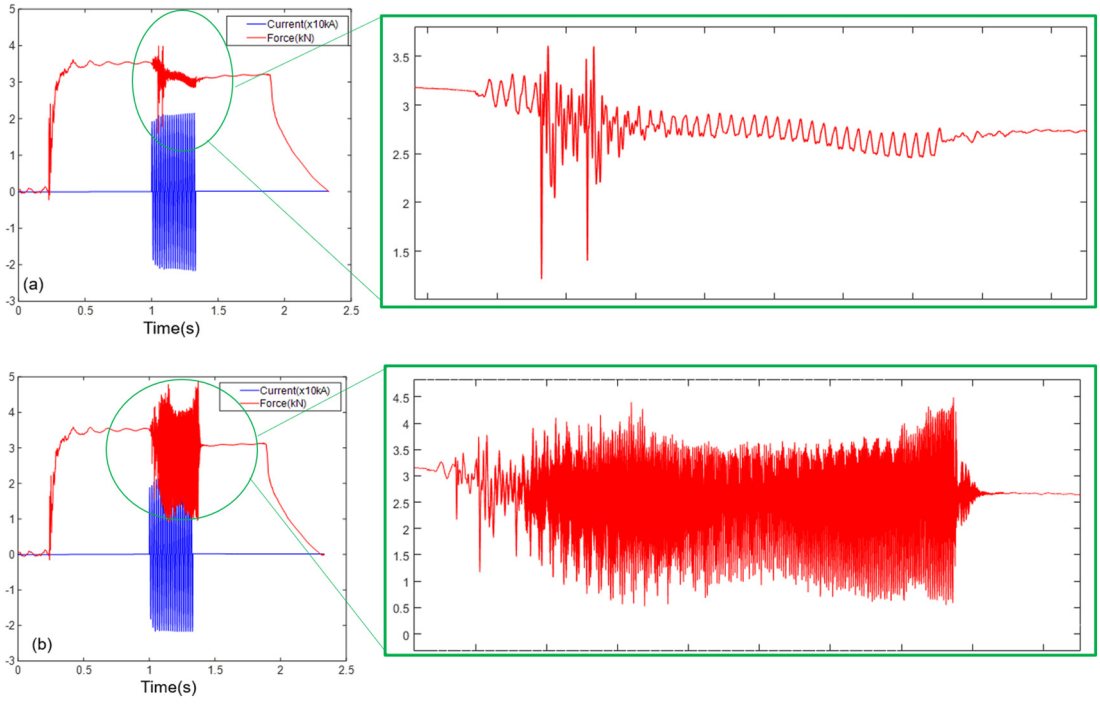


**Fig. 2.** (a) RSW Force curve at 13.4 kA & 20 cycles; (b) URW Force curve at 13.4 kA & 20 cycles.

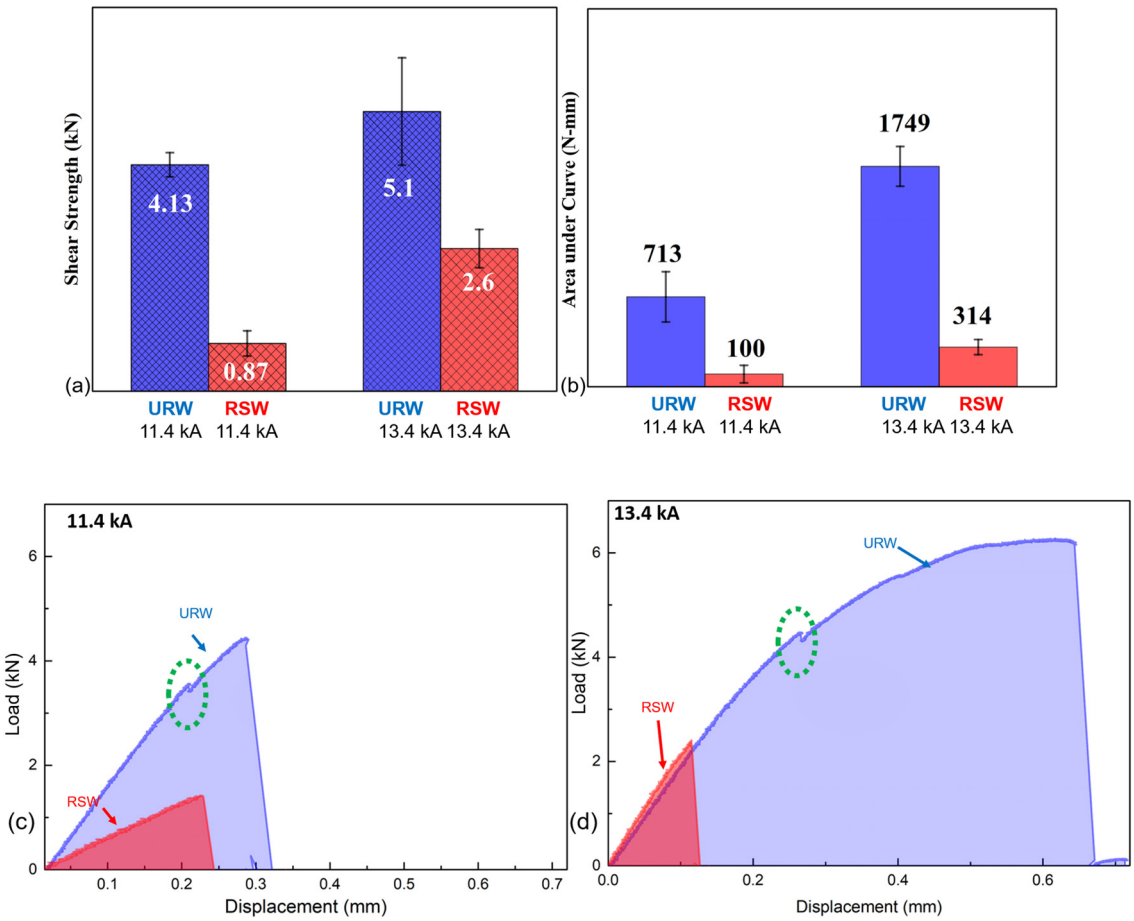


**Fig. 3.** Tensile test results (a) Joint shear strength from 11.4 kA (30 cycles) & 13.4 kA (20 cycles); (b) Energy absorption calculated via area under load-displacement curve for 11.4 kA (30 cycles) & 13.4 kA (20 cycles); (c-d) load-displacement curve for 11.4.

is observed in both URW and RSW welds. At 13.4 kA, RSW welds still showed interfacial failure mode and relatively flat fracture surface, whereas in URW welds (13.4 kA), a small pile of aluminum is attached to the steel surface, indicating much stronger bonds. Small spikes in the middle of the URW curve (Fig. 3 c&d) are potentially related to local instabilities of the bonded area. Since bonding condition and intermetallic at the micro level can vary at different locations, during tensile loading, local fracture can be initiated in some weakly bonded areas and result in a small drop of the force curve. As the applied load continues to increase, remaining area of the weld is still able to provide enough strength until the fracture propagates throughout the entire weld.

### 3.2. Weld microstructure comparison

Fig. 4 compares the optical microscopic images of RSW and URW weld cross sections. RSW welds at 11.4 kA showed point bonded region with the length of around 1177 μm. In this region, the bondline is discontinuous and the joint is created at the interface through disconnected spots, as shown in the magnified Fig. 4(a-c) highlighted with dashed blue outline. Compared with URW welds obtained at the same electrical current condition (11.4 kA for 20 cycles), the length of the fully bonded region is around 5758 μm, which is much larger than that in RSW welds. This increased bonded area contributes to the improved joint mechanical properties. Similarly, at higher current condition of 13.4 kA, URW joint shows the largest bonded length of 7129 μm, which partially explains its highest joint strength (5.1 kN) and load carrying energy (1749 N-mm). Indentation depth (ID) of the RSW welds increased from ~ 0.36 mm at 11.4 kA to ~ 0.39 mm at 13.4 kA. URW samples showed slightly higher ID compared with RSW welds, with increases of ~0.1 mm at both current conditions of 11.4 kA and 13.4 kA.

To further reveal the detailed weld interface microstructure, higher magnified SEM images are provided in Fig. 5. In conventional RSW welds, random irregular patterns of widely debonded areas occur throughout the interface (Fig. 5c and d), which is detrimental to joint integrity and leads to the low strength. At lower current of 11.4 kA, Al—Fe joint is possibly achieved through a brazing mechanism with melted Zn. Discontinuities along the interface are due to uneven thermal contraction that results in localized shrinkage and unbonded region. At higher current of 13.4 kA, zinc evaporation makes it more prone to welding defects. During RSW, initially force is applied to create a pressure zone between the electrodes. As the electrical current passes by, Joule heating rapidly increases the temperature at the interface and results in material melting. After the electrical current is stopped, the associated rapid cooling can induce solidification shrinkage. Particularly for welding aluminum to steel, their different thermal expansion coefficients and conductivities lead to a large mismatch in thermal contraction strains and induce high residual stress [13] [14]. Accordingly, cracks and debonded areas are formed at the end of the welding cycle, as observed in RSW welds of this study. Since the steel also contains a Zn coated layer, evaporation of Zn from electrical resistance heating facilitates the generation of weld crack deficiencies as well [15]. Arghavani et al. [16] studied resistance spot welding of Al-5051 to galvanized steel ASTM A653 with a zinc layer thickness of 10 μm. They

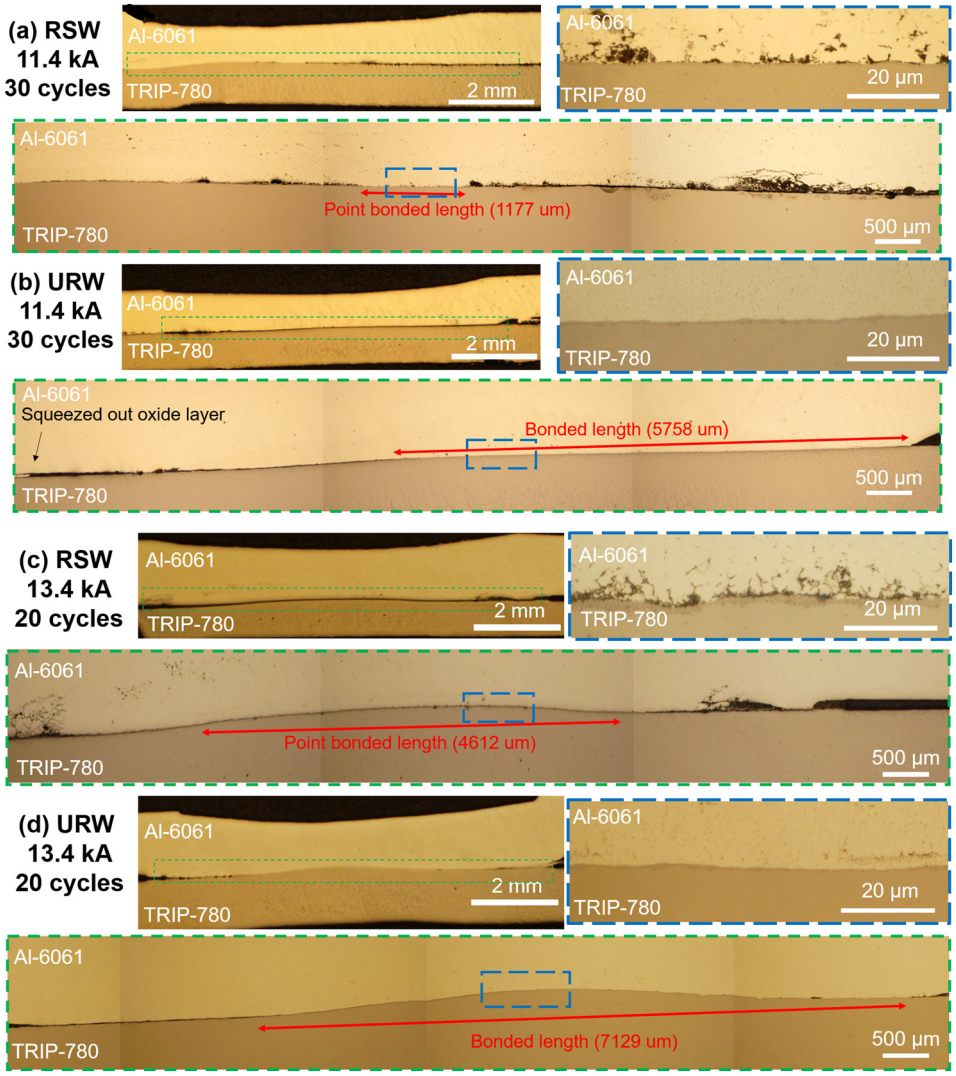


**Fig. 4.** Light optical microscope images; (a) RSW at 11.4 kA (30 cycles), (b) URW at 11.4 kA (20 cycles), (c) RSW at 13.4 kA (30 cycles) & (d) URW at 13.4 kA (20 cycles).

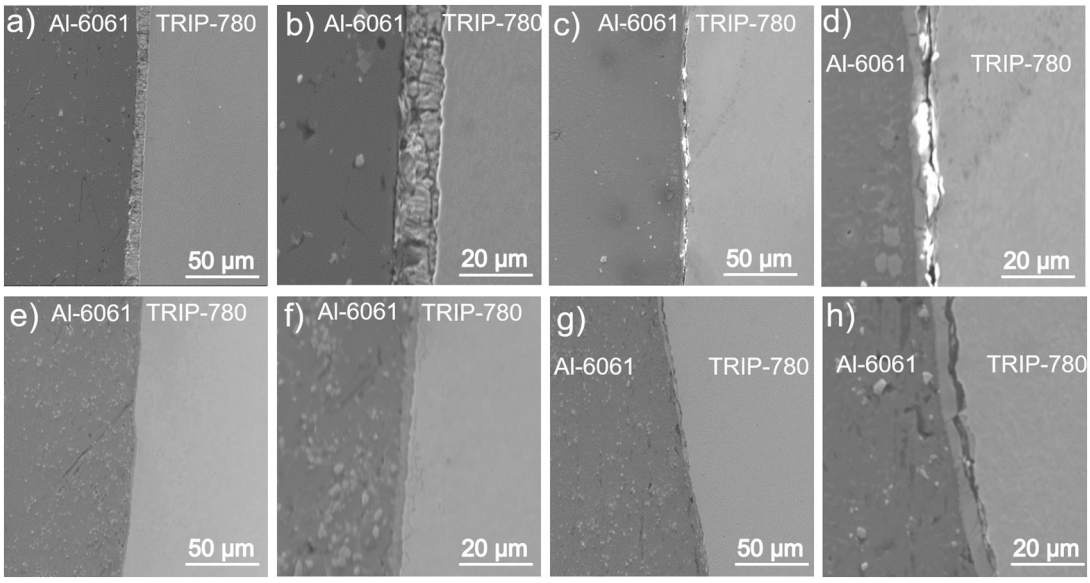


**Fig. 5.** SEM of Al-6061 & TRIP 780; (a-b) URW at 11.4 kA & 30 cycles; (c-d) RSW at 11.4 kA & 30 cycles; (e-f) URW at 13.4 kA & 20 cycles (g-h) RSW at 13.4 kA & 20 cycles. (SEM images are taken from the middle of spot weld).

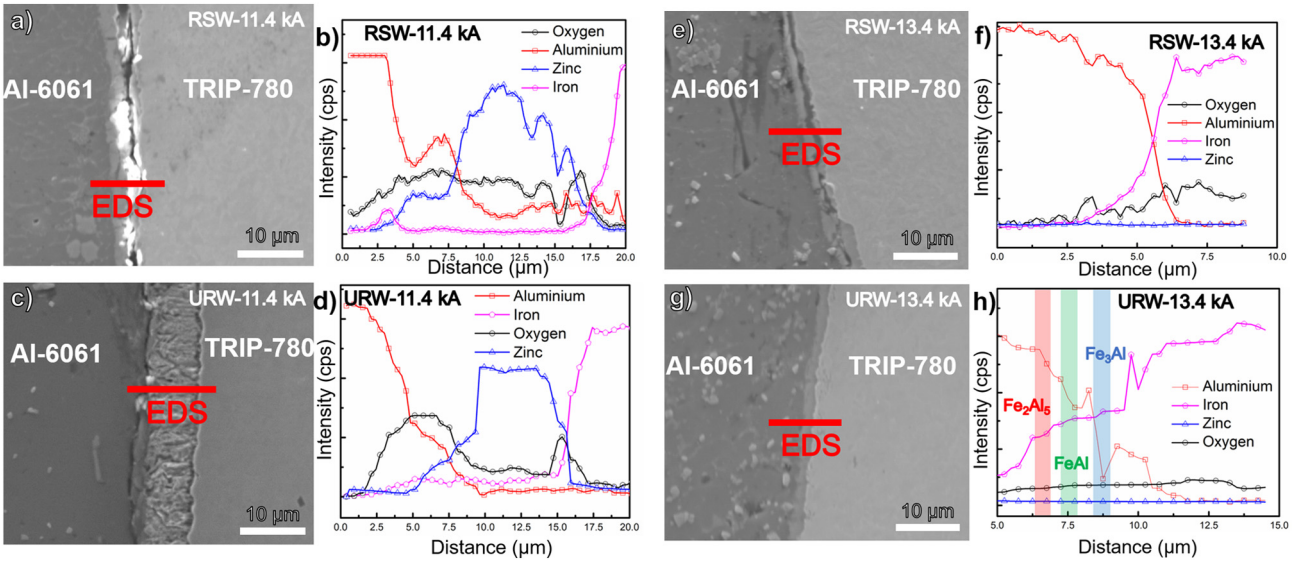


**Fig. 6.** EDS line Scan of Al-6061 & TRIP 780 across interface for RSW at 11.4 kA (a-b) & at 13.4 kA (e-f) and for URW at 11.4 kA (c-d) & at 13.4 kA (g-h).

concluded that if welding current is less than 12 kA, Zn is melted (~419 °C). Heat is consumed in the nugget and the latent heat for melting Zn is 101 kJ/kg. Above 12 kA, Zn is evaporated (~907 °C) and latent heat of Zn evaporation much higher at around 1782 kJ/kg. Evaporated zinc could result in the formation of tiny gas bubbles and also degrade the joint properties.

As a comparison, in URW welds, a continuously bonded interface is achieved. In the condition of lower current (11.4 kA) and longer weld cycles (30), an interlayer with the thickness of around 8–10 μm is observed at the Al—Fe interface, as shown in Fig. 5b. EDS line analysis revealed high amount of zinc at this layer (Fig. 6). In between the bulk aluminum and Zn layer, a thin aluminum oxide layer is observed. In this lower current condition, the Al—Fe intermetallic layer is not obvious, potentially because the weld is formed as a zinc brazed joint at the interface. It was reported that the coated Zn decreases the contact resistance, which generates less heat at the interface [17].

For URW weld obtained at higher current of 13.4 kA and 20 cycles, uniform Al—Fe intermetallic layer is observed. The Zn is not noticeable at the interface. However, EDS analysis reveals existence of Zn at the edge of the weld nugget. This is probably because the higher magnitude of current increases nugget temperature. The melted Zn is then squeezed out from the weld center towards the edge under the electrode compression force. The EDS line analysis showed existence of intermetallics across the interface with the thickness varies from 2.6 μm to 3.4 μm. According to the Al—Fe phase diagram [18], there are potentially three types of Al—Fe intermetallics formed at the interface, including $Fe_2Al_5$, FeAl and $Fe_3Al$. Chen et al. [19] classified the Al—Fe RSW joint failure modes based upon thickness of intermetallic layer. He concluded that the intermetallic (IMC) layer with thickness of less than 3 μm will result in button pullout mode while the IMC layer of thickness greater than 3 μm, interfacial debonding failure occurs. This agrees with the mixed failure mode observed on fracture surfaces of our URW welds obtained at 13.4kA

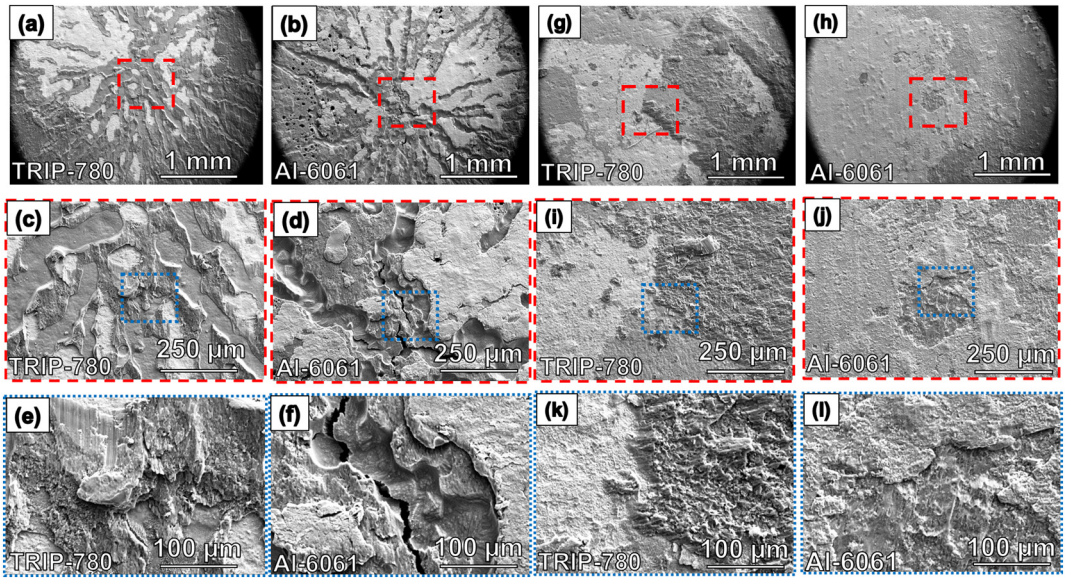


**Fig. 7.** (a-f) SEM of fracture surface after tensile testing RSW at 11.4 kA & 30 cycles; (a), (c) & (e) corresponds to TRIP-780 fracture surface whereas (b), (d) & (f) corresponds to Al-6061 surface after fracture; (g-i) URW at 11.4 kA & 30 cycles; (g), (i) &(k) corresponds to TRIP-780 fracture surface whereas (h), (j) & (l) corresponds to Al-6061 surface after fracture.

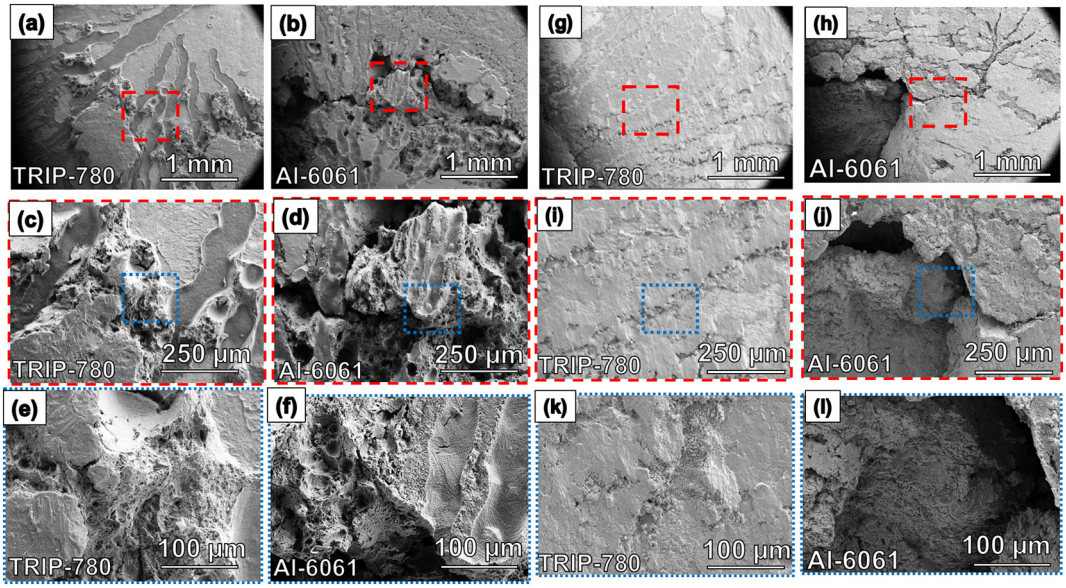


**Fig. 8.** (a-f) SEM of fracture surface after tensile testing RSW at 13.4 kA & 20 cycles; (a), (c)&(e) corresponds to TRIP-780 fracture surface whereas (b), (d) & (f) corresponds to Al-6061 surface after fracture; (g-i) URW at 13.4 kA & 20 cycles; (g), (i)&(k) corresponds to TRIP-780 fracture surface whereas (h), (j) & (l) corresponds to Al-6061 surface after fracture.

(Fig. 8), where thickness of the IMC layer varies from 2.6 μm to 3.4 μm across the Al—Fe interface.

Figs. 7 & 8 compared fractured surface of the RSW and URW joints after lap shear tensile tests obtained from different electrical conditions. In the case of 11.4 kA with 30 cycles, RSW samples (Fig. 7a-f) are dominated with highly brittle cleavage features, whereas in URW samples (Fig. 7g-l), some dimpled fracture surface with cup and cone features are observed, indicating relatively ductile behavior. At 13.4 kA condition, RSW samples (Fig. 8a-f) also showed brittle appearance (8e) whereas URW welds fracture surface contained both brittle and ductile failure characteristics (Fig. 8g-l).

Fractured surface of RSW welds are examined in more details and results are shown in Fig. 9. Eggcrate features are observed under both 11.4 kA and 13.4 KA conditions, which are typical features of solidification cracking [20]. These also correspond to the observed unbonded area in the previous weld cross section microstructure, which directly deteriorate the Al—Fe RSW joint quality and lead to brittle failure mode with low strength. Fig. 10 (a-b) shows the direct evidence of solidification cracking inside the

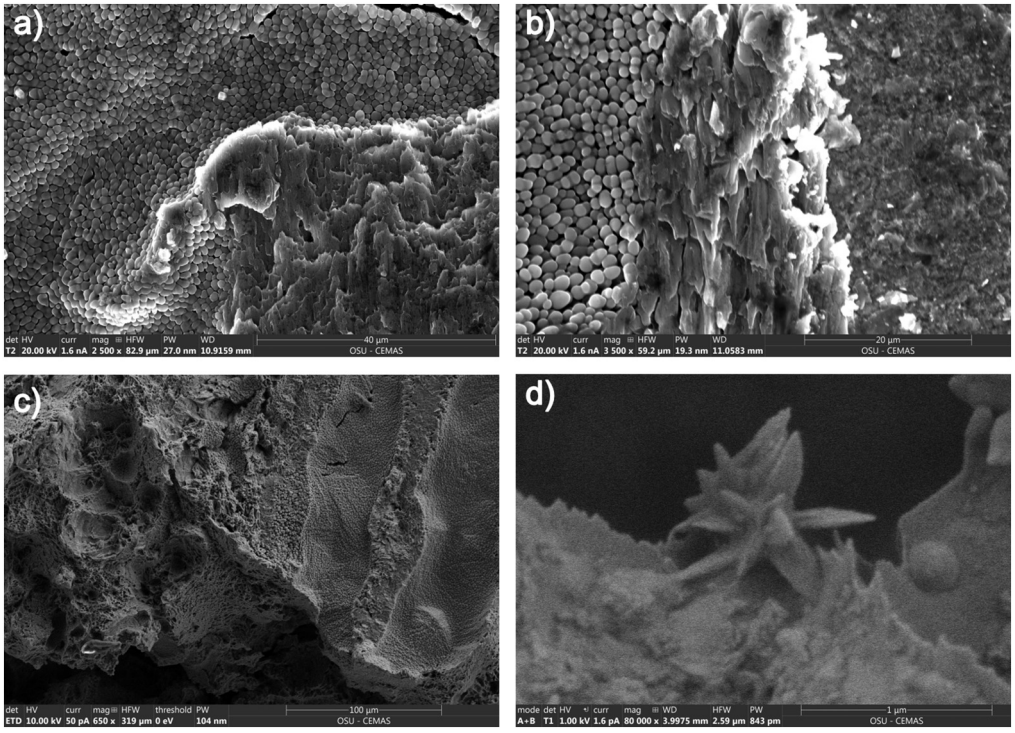


**Fig. 9.** (a&b) Fracture surface for RSW at 11.4 kA c) Fracture surface for RSW at 13.4 kA. d) The periphery of fracture surface for RSW at 13.4 kA indicates the presence of zinc oxide flowers or Fe—Al intermetallics.

unbonded region of RSW joints, represented by the typical rounded edges in Fig. 10 (b). This morphology is more obvious on the fractured surface of RSW joints, as shown in Fig. 10 (c). Eskin [21] summarized mechanisms of solidification cracking, which include thermal contraction, liquid film rupture, liquid pressure drop and vacancy supersaturation. As a comparison, fractured surface of the URW joints showed some ductile dimple features (Fig. 10 d-e). In liquid, ultrasonic energy produces various nonlinear effects such as cavitation and acoustic streaming, which help in the minimization of solidification defects. In the later stage when material is solidified, ultrasonic energy induces oscillating stress fields, which increases the concentration of dislocations and point defects up to certain saturation level, followed by the formation of new refined grains [22]. Zhang et al. [23] reported that ultrasonic energy can alter the fluidity pattern of the aluminum melt that improves wettability, enhances dispersion of oxide inclusions in the melt and promotes grain refinement. He also mentioned that ultrasonic energy minimizes the thermal contraction, which is one of the main reasons of solidification cracking.

Fig. 11(a&b) shows a schematic model that explains the possible effects of ultrasonic vibration on RSW process. As the electrical current passes through pressure zone during RSW process, localized melting takes place at the interface followed by inward solidification. A mushy zone exists ahead of solidification front, which is the most susceptible region to cracking due to the liquation. Another region prone to cracking is the interdendritic area, where filling of the material solely depends upon the presence of remaining liquid metal. During solidification, penetration through the solidified dendrites becomes more difficult for the liquid metal. Besides, the semi-solid nature of the mushy zone hinders the flow of liquid metal, which facilitate cracks propagation. Ultrasonic vibration can alleviate these aforementioned problems by adding disturbance material flow from the acoustic streaming and cavitation effects. This flow breaks down the dendrite fragments (Fig. 11b-Stage B), creates additional nucleation sites and promotes epitaxial structure growth during URW process. Moreover, ultrasonic vibration enhances the flowability of the liquid metal in the mushy zone. Another potential ultrasonic effect is to homogenize element distribution in the liquid metal, which minimizes element segregation and also reduces possibility of solidification cracking.

### 3.3. Ultrasonic effects on RSW process

For a further understanding of the hybrid URW process, in situ observation of ultrasonic vibrations during URW is achieved via a high-speed camera (Photron SA-X2) under the image capturing rate of 100,000 frames per second (100 k fps). In the setup, the stack of aluminum and steel sheet is placed halfway at the center of the electrode. An edge weld is performed, as shown in Fig. 12.

From the high-speed imaging, ultrasonic effects can generally be described in two categories, depending on the occurrence of melting. In conditions without melting as shown in Fig. 13, ultrasonic vibration helps abrade of surface oxides and asperities. The break-up particles are marked with red circles in Fig. 13. This modifies the contact conditions between the two sheets, and accordingly the resistance heat generation rate. If melting occurs, as shown in Fig. 14, the ultrasonic waves promote wetting of melted aluminum with steel, facilitate spreading of the locally melted spot and create a uniformly melted interlayer.

Based on these observations, it is hypothesized that ultrasonic vibration can alter the RSW process dynamics at several stages. At the beginning of the weld cycle, reduced contact resistance can be achieved as the ultrasonic vibration breaks off the surface oxide layer and removes undesirable contaminants at the faying surfaces of the two workpieces. Since the actual geometry of the electrode is not ideally flat, relative shear components can be expected at the steel aluminum interface even though the ultrasonic vibration is perpendicularly configured. In addition, acoustic softening [24] of the material enhances the plastic deformation under electrode force. As a result, net contact area between the two workpiece increases by closing the initial gaps. All these effects can reduce contact resistance and lower the heat generation rate. This potentially explains the perseverance of Zn layer at the Al—Fe interface in the URW welding condition of 11.4 kA.

In the middle of the weld cycle, if melting occurs, the ultrasonic vibration would influence material flow dynamics in the melt pool, as shown in the high-speed video. The alternate compression and rarefaction field from ultrasonic vibrations can induce cyclic stresses into the joint. This alters the solidification pattern of welding process by detachment of dendritic fragments ahead of solidification front, which serves as addition nucleation sites,

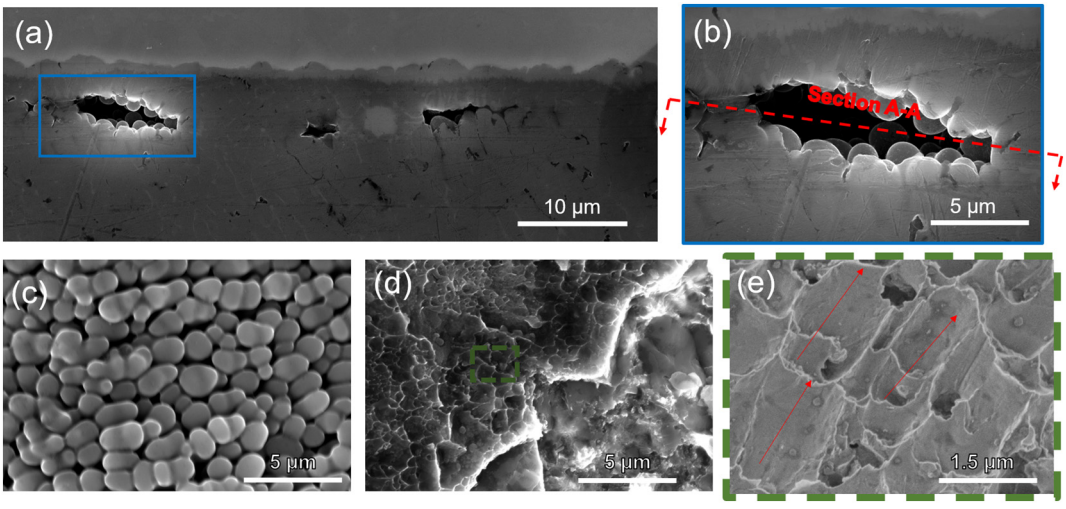


**Fig. 10.** (a-b) Solidification cracks in RSW welds. (c) Characteristic image of solidification cracking as seen on the fractured surface for RSW joint. (It can be interpreted as the top view of the Section A-A) (d) SEM of fractured surface for URW joints. (e) Magnified view of ductile dimples appeared on the fractured surface of URW joints. Arrows indicate the direction of the dimples elongated in the shear direction.

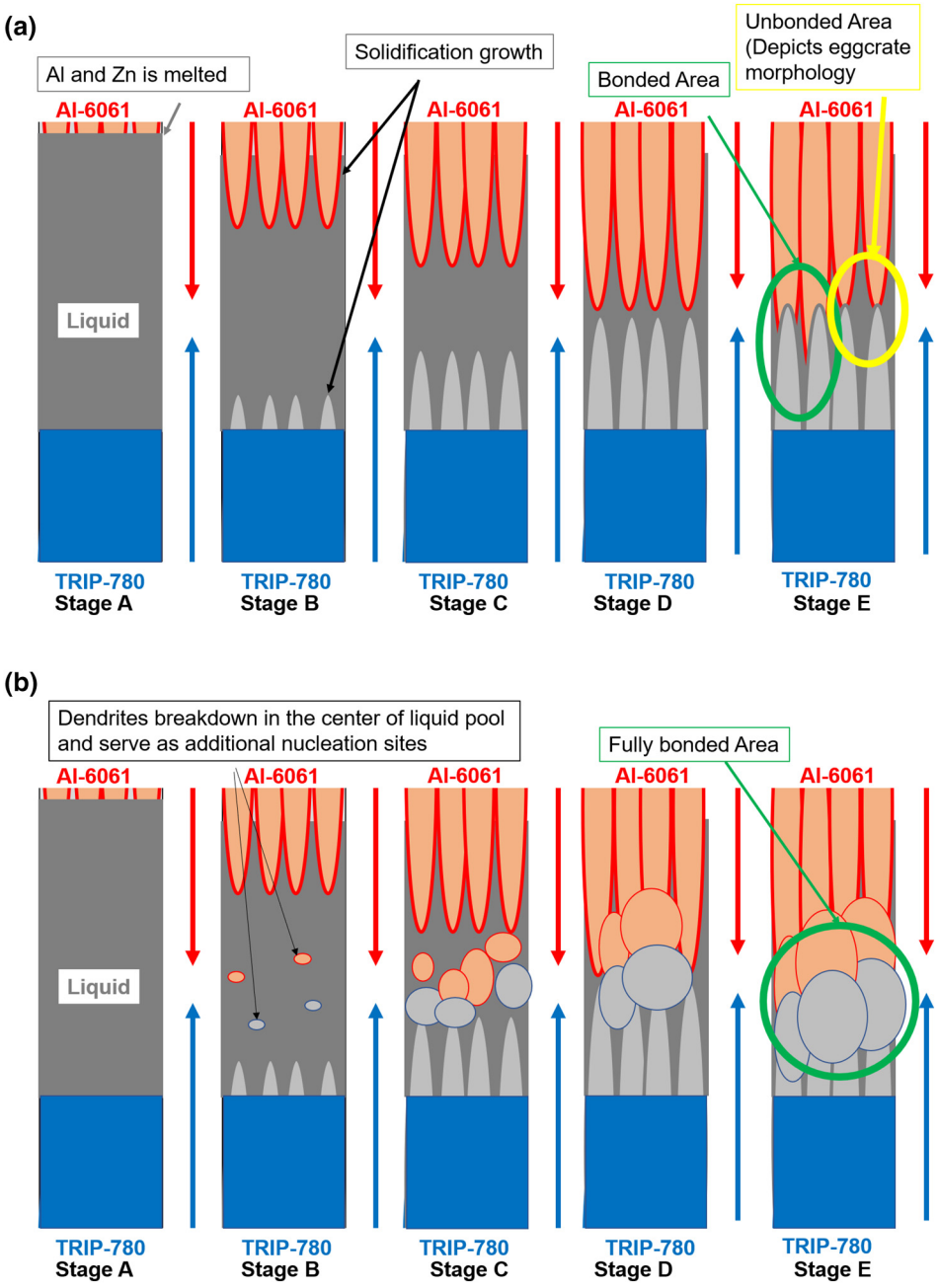


**Fig. 11.** a. Schematics of solidification process during RSW. b. Schematics of solidification process during URW.

facilitates bonding and minimizes the overall solidification cracking. At the end of the weld cycle, ultrasonic cavitation effects can minimize possible shrinkage porosities [25], which is similar to the mechanisms of ultrasonic degassing.

Finally, during cooling down, the acoustic softening effect [24] helps ameliorate thermal stresses and maintains bonding at the Al—Fe interface. However, continuing supply of ultrasonic energy for a long period can potentially induce fatigue failure and generate cracks at the nugget edge, which becomes undesirable.

## 4. Conclusions

1) The hybrid URW process significantly improves the load-bearing capacities of Al6061-TRIP780 steel welds from conventional RSW.
2) The superimposed ultrasonic energy promotes bonding formation at the Al—Fe interface, increases the bonded area and removes the interfacial cracks that are generally observed in conventional RSW welds.
3) The URW welding force curves show frequencies of both ultrasonic vibration and AC current cycles.
4) Ultrasonic vibration facilitates breakdown of the surface oxide and contaminants, which modifies contact resistance and heat generation rate. If melting occurs, ultrasonic vibration promotes wetting of the molten aluminum over the steel interface and modifies the material flow dynamics in the melt pool.

The proposed hypothesis of ultrasonic effects on RSW process will be verified in details in future works.

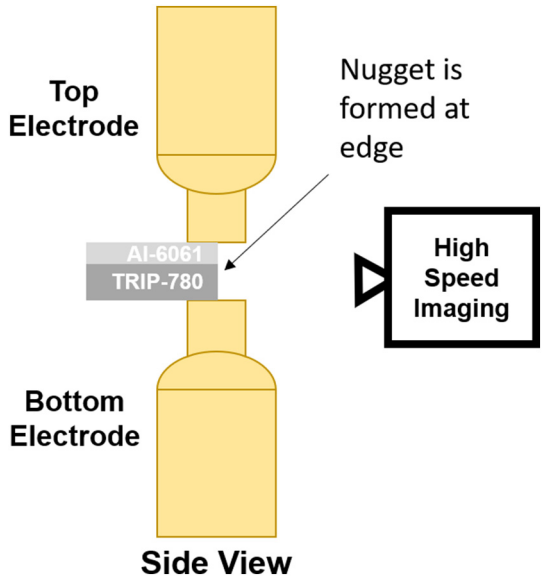


**Fig. 12.** Electrode-workpiece assembly for High Speed Imaging.

## Data availability statement

The raw/processed data required to reproduce these findings cannot be shared at this time due to technical or time limitations.

## CRediT authorship contribution statement

**Umair Shah:** Conceptualization, Formal analysis, Funding acquisition, Investigation, Methodology, Project administration, Resources, Supervision, Writing - review & editing. **Xun Liu:** Conceptualization, Formal analysis, Funding acquisition, Investigation, Methodology, Project administration, Resources, Supervision, Writing - review & editing.

## Acknowledgements

Authors would like to thank Matt Short from Edison Welding Insititue for his assistance in tuning ultrasonic devices, Mai Huang from Arcelormittal for providing the TRIP steel sheets. Microstructure characterization works are supported by the OSU IMR grant 'Ultrasonic resistance spot welding of dissimilar materials'. The project is supported by National Science Foundation under the grant No. 1853632, An Innovative Hybrid Ultrasonic Resistance Welding Process for Joining Advanced Lightweight and Dissimilar Materials.

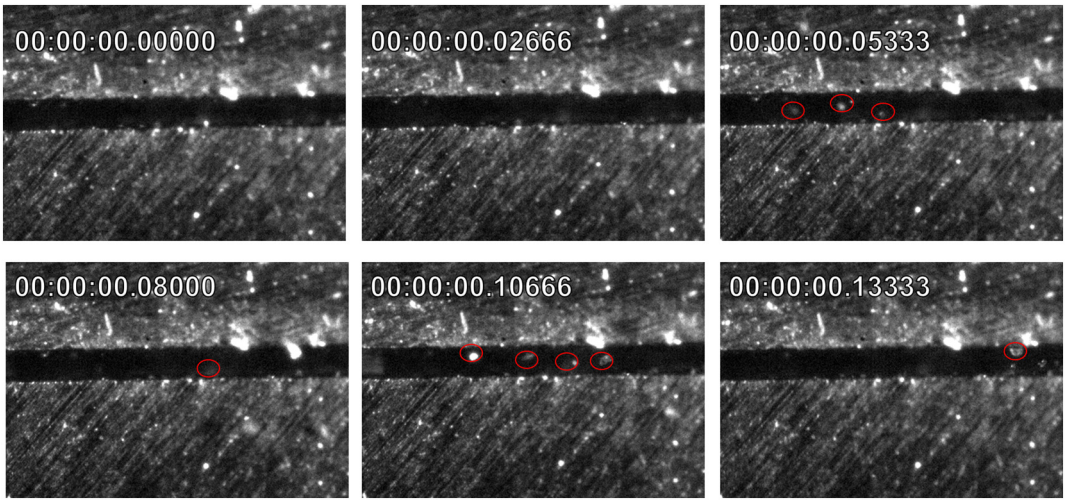


**Fig. 13.** High-Speed Imaging at the Al—Fe interface showing breakdown of surface oxide layer and asperities during URW process. Red circles indicate particles breakdown process during URW process. (For interpretation of the references to colour in this figure legend, the reader is referred to the web version of this article.)

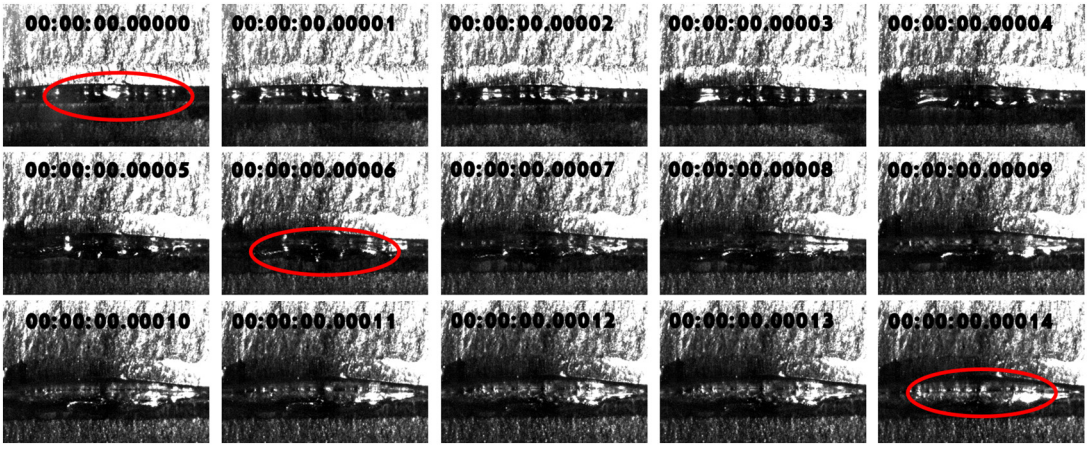


**Fig. 14.** High Speed Imaging at the Al—Fe interface showing wetting of aluminum during URW process. Highlighted circle indicates molten aluminum.

## References


[1] J. Chen, X. Yuan, Z. Hu, C. Sun, Y. Zhang, Y. Zhang, Microstructure and mechanical properties of resistance-spot-welded joints for A5052 aluminum alloy and DP 600 steel, Mater. Charact. 120 (2016) 45–52, https://doi.org/10.1016/J.MATCHAR.2016.08.015.

[2] W. Zhang, D. Sun, L. Han, Y. Li, Optimised design of electrode morphology for novel dissimilar resistance spot welding of aluminium alloy and galvanised high strength steel, Mater. Des. 85 (2015) 461–470, https://doi.org/10.1016/J.MATDES.2015.07.025.

[3] N. Sigler, D.R. Carlson, B.E. Wang, H.-P. Chen, Multistep Electrode Weld Face Geometry for Weld Bonding Aluminum to Steel, https://patents.google.com/patent/CN107520550A/en 2017, Accessed date: 10 August 2018.

[4] R. Qiu, C. Iwamoto, S. Satonaka, Interfacial microstructure and strength of steel/aluminum alloy joints welded by resistance spot welding with cover plate, J. Mater. Process. Technol. 209 (2009) 4186–4193, https://doi.org/10.1016/J.JMATPROTEC.2008.11.003.

[5] D. Bakavos, P.B. Prangnell, Mechanisms of joint and microstructure formation in high power ultrasonic spot welding 6111 aluminium automotive sheet, Mater. Sci. Eng. A 527 (2010) 6320–6334, https://doi.org/10.1016/J.MSEA.2010.06.038.

[6] F. Haddadi, Rapid intermetallic growth under high strain rate deformation during high power ultrasonic spot welding of aluminium to steel, Mater. Des. 66 (2015) 459–472, https://doi.org/10.1016/J.MATDES.2014.07.001.

[7] B.J. Ruszkiewicz, L. Mears, J.T. Roth, Investigation of heterogeneous joule heating as the explanation for the transient electroplastic stress drop in pulsed tension of 7075-T6 aluminum, J. Manuf. Sci. Eng. 140 (2018), 091014. https://doi.org/10.1115/1.4040349.

[8] X. Liu, S. Lan, J. Ni, Experimental study of electro-plastic effect on advanced high strength steels, Mater. Sci. Eng. A 582 (2013) 211–218, https://doi.org/10.1016/J.MSEA.2013.03.092.

[9] Xu Guocheng, Jing Wen, C. Wang, Xiaoqi Zhang, Quality monitoring for resistance spot welding using dynamic signals, 2009 Int. Conf. Mechatronics Autom, IEEE 2009, pp. 2495–2499, https://doi.org/10.1109/ICMA.2009.5246513.

[10] U.I. Chang, J. Frisch, On optimization of some parameters in ultrasonic metal welding, Weld. J. (1974)https://doi.org/10.1016/j.agsy.2016.05.003.

[11] Q. Mao, J.M. Gibert, G. Fadel, Investigating ultrasound-induced acoustic softening of aluminum 6061, 26th Conf. Mech. Vib. Noise, vol. 8, ASME, 2014https://doi.org/10.1115/DETC2014-34579 , p. V008T11A100.

[12] J.A. Gallego-Juárez, K.F. Graff, Power Ultrasonics: Applications of High-Intensity Ultrasound, Woodhead Publishing, 2015https://doi.org/10.1016/B978-1-78242-028-6.00001-6.

[13] H. Zhang, J. Senkara, X. Wu, Suppressing cracking in resistance welding AA5754 by mechanical means, J. Manuf. Sci. Eng. (2002)https://doi.org/10.1115/1.1418693.

[14] J. Sankara, H. Zhang, Crackin g in spot welding aluminum alloy AA5754, Weld. Res. (Suppl) (2000) 194–201https://app.aws.org/wj/supplement/WJ_2000_07_s194.pdf.

[15] K. Luboš, J. Viňáš, R. Mišičko, Influence of welding current in resistance spot welding on the properties of Zn coated steel DX51D, Songklanakarin J. Sci. Technol. 38 (2016) 237–242.

[16] M.R. Arghavani, M. Movahedi, A.H. Kokabi, Role of zinc layer in resistance spot welding of aluminium to steel, Mater. Des. 102 (2016) 106–114, https://doi.org/10.1016/J.MATDES.2016.04.033.

[17] H. Zhang, J. Senkara, J. Senkara, Resistance Welding, CRC Press, 2011https://doi.org/10.1201/b11752.

[18] J. Song, T. DenOuden, Q. Han, Mechanisms of soldering formation on coated core pins, Metall. Mater. Trans. A. 43 (2012) 415–421, https://doi.org/10.1007/s11661-011-0865-y.

[19] N. Chen, H.-P. Wang, B.E. Carlson, D.R. Sigler, M. Wang, Fracture mechanisms of Al/steel resistance spot welds in lap shear test, J. Mater. Process. Technol. 243 (2017) 347–354, https://doi.org/10.1016/J.JMATPROTEC.2016.12.015.

[20] J.C. Lippold, Welding Metallurgy and Weldability, John Wiley & Sons, Inc, Hoboken, NJ, 2015https://doi.org/10.1002/9781118960332.

[21] D.G. Eskin, L. Katgerman, A Quest for a New Hot Tearing Criterion, (n.d.). doi:https://doi.org/10.1007/s11661-007-9169-7.

[22] Q. Han, Ultrasonic processing of materials, Metall. Mater. Trans. B Process Metall. Mater. Process. Sci. 46 (2015) 1603–1614, https://doi.org/10.1007/s11663-014-0266-x.

[23] L. Zhang, Ultrasonic Processing of Aluminum Alloys | TU Delft Repositories, TUDelft 2013https://doi.org/10.4233/uuid:6bb7c382-3f25-4a64-b3f4-8a08da229185.

[24] J. Prakash, A review on solidification and change in mechanical properties under vibratory welding condition, Int. J. Eng. Sci. (2010)https://doi.org/10.1059/0003-4819-3-5-495.

[25] G.I. Ėskin, Ultrasonic Treatment of Light Alloy Melts, CRC Press, 2017.